Bulletin of Volcanology (2025) 87:83
https://doi.org/10.1007/s00445-025-01868-3

RESEARCH ARTICLE

Effervescent fountaining—a transition between explosive and lava-dome forming eruptions: evidence from "boiling-over" pyroclastic flows from the March 2019 eruption of Bezymianny volcano, Kamchatka

Andreas Auer[1] · Thomas R. Walter[2] · Lea Ostorero[3] · Alexander Belousov[4] · Marina Belousova[4] · Hélène Balcone-Boissard[5] · Georges Boudon[6] · Rene Mania[2] · Alina V. Shevchenko[2]

Received: 17 March 2025 / Accepted: 22 August 2025

Abstract

Pyroclastic density currents (PDCs) are a major volcanic hazard, whose variability of triggering and deposition mechanisms suggests highly complex and different initial states to be considered. Here, we describe block and ash flow deposits from the March 2019 eruption of Bezymianny volcano, Kamchatka. Ash clouds from this eruption extended into the Pacific Ocean, while block and ash flow deposits were found widely across the slopes of the edifice. We use satellite and drone-based photogrammetry to show material dispersal and accumulation during the eruption. We also use these photogrammetric data to obtain basic granulometry, suggesting dominantly 60 cm block dimensions, some exceeding 2 m in scale, embedded in a fine ash matrix. In addition, we sampled the deposit and herein demonstrate how distinct petrographical features can be used to distinguish the type of block and ash flow. Deposit characteristics, density, dimension, and petrography suggest that PDC initiation occurred during an eruptive episode conventionally considered as a "boiling over" event. This activity is characterized by rapid magma volume expansion due to intense gas exsolution which is driving a frothed mass out of the vent leading to the formation of large but highly vesicular juvenile blocks. Such an eruption style is transitional between effusive (lava dome forming) and explosive activity, and we suggest a new term "effervescent fountaining" to replace the term "boiling over" as a more appropriate description of such an eruption. Material dispersal, density of juvenile material, and Fe-Ti mineralogy are useful features to distinguish different types of block and ash flow deposits. These characteristics are also applicable to deposits from eruptions and deposits within the prehistoric geological record, improving our understanding of historic eruption patterns.

Keywords Lava dome · Boiling over pyroclastic flow · Block and ash flow · Pyroclastic density current (PDC) · Bezymianny volcano · Effervescent fountaining

Editorial responsibility: M. Edmonds

✉ Andreas Auer
auer@riko.shimane-u.ac.jp

[1] Department of Geoscience, Shimane University, 1060 Nishikawatsu, Matsue 690-8504, Japan

[2] GFZ Helmholtz Centre for Geosciences, Telegrafenberg. Potsdam 14473, Germany

[3] Department of Earth and Environmental Sciences - DISAT, University of Milano-Bicocca, Piazza Dell'Ateneo Nuovo, Milan 1 - 20126, Italy

[4] Institute of Volcanology and Seismology, Petropavlovsk-Kamchatsky, Russia

[5] Institut Des Sciences de La Terre de Paris (ISTeP), Sorbonne Université, CNRS, 4 Place Jussieu, Paris 75005, France

[6] Université Paris Cité, Institut de Physique du Globe de Paris (IPGP), CNRS, 75005 Paris, France

Published online: 13 September 2025

Introduction

The majority of volcanic eruption styles is named after a volcano where a specific eruption type is common (Walker 1973). However, a single specific eruption style is not necessarily tied to any individual volcano (Bevilacqua et al. 2020), and many volcanoes exhibit varying magnitudes and eruption styles over short timeframes (Ruprecht et al. 2012; Auer et al. 2016; Boudon and Balcone-Boissard 2021). A notable exception is so called "boiling over" eruptions, a term that, despite being an obvious misnomer, has been kept in the volcanological literature for more than 150 years, not only as a vivid description of the activity around the active vent but also as a key initiation mechanism for pyroclastic density currents (PDCs) (Dufek et al. 2015). Pyroclastic density currents are fast-moving, ground-hugging flows of particulate-fluid mixtures that travel down the slopes of a volcano. They are driven by gravity and can reach speeds of over 100 km/h and temperatures of several hundred degrees Celsius (Sulpizio et al. 2014). Transportation and depositional mechanisms of PDCs are usually deduced from deposit characteristics (Branney et al. 2002), computational modelling (Dufek 2016), and analog experiments (Lube et al. 2015, 2019; Walding 2022).

Several mechanisms (Fig. 1) are considered for the initiation of pyroclastic density currents (Dufek et al. 2015): Lateral blasts (Fig. 1a) result from laterally (sometimes vertically) directed explosive decompression of lava domes and shallow cryptodomes (Belousov et al. 2007). The resultant dilute and turbulent PDCs do usually not produce large volume deposits (0.2–0.4 km^3 in case of Bezymianny 1956); the maximum grain size is small compared to block and ash flow deposits (see below), and the overall grain size distribution is more restricted. In lateral blasts, inertial forces will

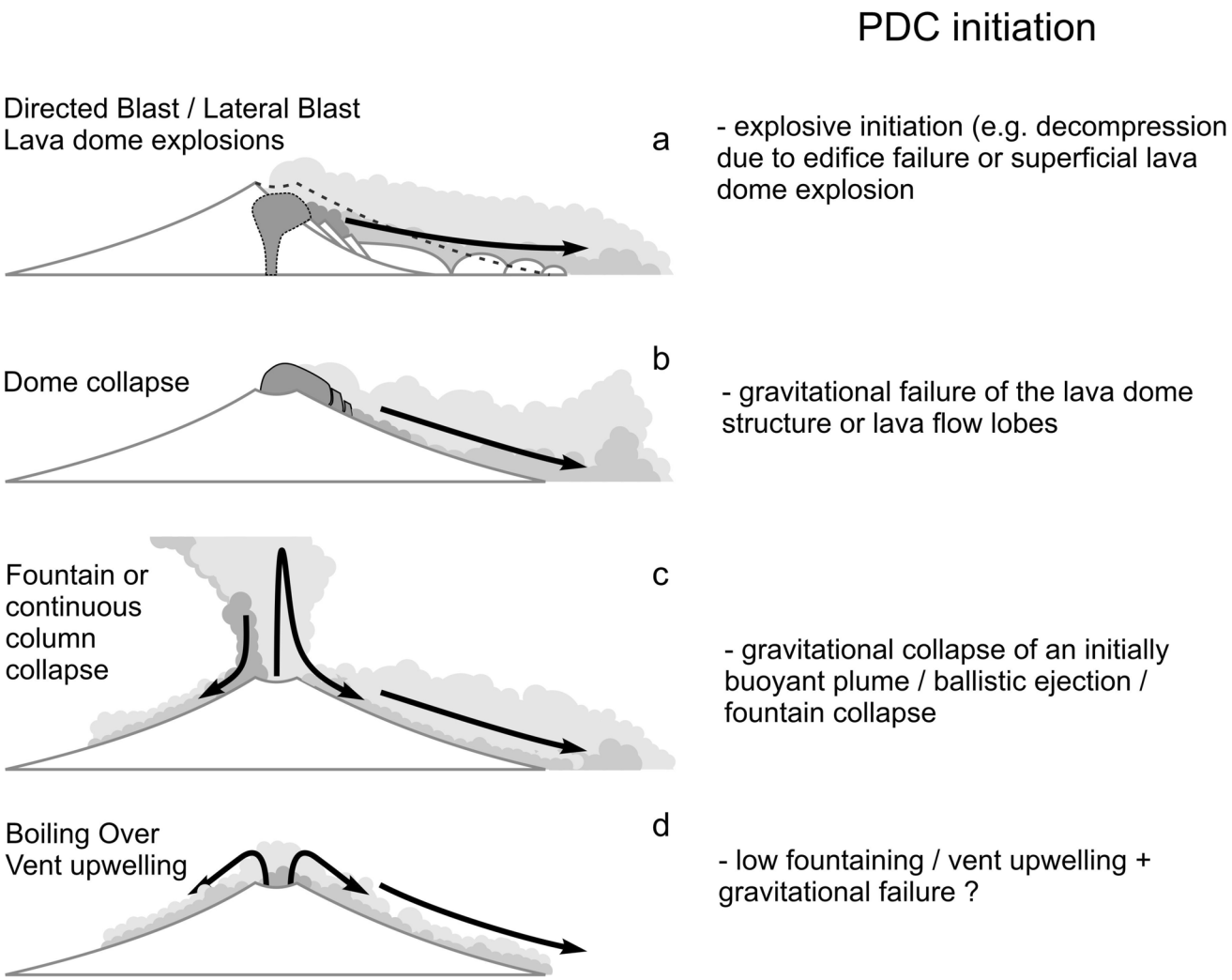

Fig. 1 Initiation mechanisms for pyroclastic density currents, modified after Dufek et al. (2015)

initially dominate over gravitational forces and can therefore inundate large areas relatively unconstrained by topography and present a substantial hazard usually for a specific sector around the volcano (Crandell and Hoblitt 1986; Belousov 1996). Dilute pyroclastic density currents also form during directed superficial explosions of growing lava domes, especially during the early stages of dome-forming eruptions. Such events are similar to directed blasts and marked, for example, the beginning of the 1902 eruption of Montagne Pelée, Martinique (Boudon and Lajoie 1989; Boudon et al. 1990, 2015).

Gravitational collapses of growing lava domes (Fig. 1b) can generate pyroclastic density currents (Calder et al. 2015). During the last 40 years, they have been studied in great detail at several active volcanoes around the world (Ui et al. 1999; Charbonnier and Gertisser 2008; Krippner et al. 2018; Nakada et al. 2019). The resulting pyroclastic density currents are typically block and ash flows (BAF). This term has become synonymous with lava dome eruptions, and Calder et al. (2015) even define block and ash flows as "the deposits of pyroclastic density currents generated by lava dome collapse." However, their review subsequently states that block and ash flows are also formed during intermittent explosive episodes. Since the term "BAF" is purely descriptive, usually referring to the pronounced bimodal grain size distribution of the deposits (Sarocchi et al. 2011), it can be misleading to tie the definition of the term solely to lava dome collapse events, and while most dome collapse processes will produce BAF deposits, not all BAF deposits result from dome collapse processes) as will be discussed in this work.

Eruption column collapse and fountaining (fountain collapse) are considered other fundamental processes during which pyroclastic density currents initiate. The simplified model by Dufek et al. (2015) shown in Fig. 1c is subdivided by several authors into different subcategories (Cas and Wright 1987), of which the most important ones are discrete single pulse collapse (producing a highly unsteady current) and continuous sustained fountaining (producing quasi steady currents) (Branney et al. 2002). While single pulse collapse is often associated with Vulcanian style activity (Cole et al. 2002; Druitt et al. 2002), continuous sustained fountaining originates directly from the interior parts of gas-thrust jets, where part of the particulate dispersion loses momentum, fails to become buoyant, and follows fountain-like trajectories to the ground (Sparks et al. 1997; Branney et al. 2002). Further subdivision and classification of PDC deposits from eruption column collapse have been attempted depending on the size and style of the eruption (Giordano and Cas 2021) and the source and initiation of the current (Cole et al. 2002).

Another mechanism usually considered for the initiation of pyroclastic density current is called "boiling over type" (Fig. 1d). This type has intermediate energy between lava dome failure and column collapse (Dufek et al. 2015) and occurs when frothed magma either fountains over the crater rim without forming a convective plume or reaches (and breaches) the crater rim as a frothed gas pyroclast mass within the open vent.

The term was introduced during a report on a historical eruption of Cotopaxi volcano in 1877 in reference to the description of such an event as a "boiling over pot of rice that overwhelmed the crater walls on all sides" (Wolf 1878). The historical account by Wolf (1878) describes the event as a "lava eruption" but it is evident that the transport mechanism is that of a density current as "glowing liquid lava cascaded down the slopes of the mountain with tremendous velocity" (a full translation of the "boiling over" event at Cotopaxi (Wolf 1878) can be found as Electronic Supplement S1). Boiling over type eruptions have further been observed at Mt. St. Helens (Lipman and Mullineaux 1981) and the most up-to-date direct observation, including a detailed characterization of the deposit, comes from the 2006 Tungurahua eruption (Benage et al. 2014; Dufek et al. 2015; Rader et al. 2015). We notice that the term "boil over" has also been used as a model explanation for the eruption of extensive ignimbrite deposits (e.g., Cerro Galán) lacking substantial Plinian Fall layers due to reduced admixing of air and de-densification (Sparks et al. 1978, 1985; Branney et al. 2002). Such Ultraplinian eruptions are not further considered here.

Here, we describe depositional and petrographic characteristics of PDC deposits formed during an eruptive episode at Bezymianny volcano (Kamchatka) in March 2019. This volcano has shown a large range of eruptive styles ranging from lava flows, dome forming episodes, sub-Plinian to Plinian eruptions, and cryptodome intrusion, including a sector collapse event in 1956 (Shevchenko et al. 2020). While there is no direct observational account of the March 2019 event, we use field observations, satellite, and unmanned aerial vehicle (UAV) data to characterize the deposits. In addition, we use deposit characteristics and compare petrography and textures of the products with those from the currently active lava dome. These data are used to interpret the eruption mechanism of the event (i.e., effusive vs. explosive) and suggest possible PDC initiation mechanisms (i.e., dome collapse vs. "boiling over"). Lava domes are often ephemeral geological features, and we also discuss how different types of block and ash flow deposits can be recognized and distinguished in the geological record.

Geological background

Bezymianny (2886 m above sea level) is an andesitic, dome-building composite volcano that is part of the Klyuchevskoy volcanic group in the Central Kamchatka Depression

(Bogoyavlenskaya et al. 1991; Shevchenko et al. 2020). Between 2.4–1.7 ka and 1.35–1 ka BP, major eruptive activity occurred at Bezymianny (Braitseva et al. 1991). The prehistoric eruptive activity formed lava flows, lava domes, and extensive pyroclastic density current deposits, with magma compositions ranging from basalt to andesite, and volcanic activity preceded by long phases of dormancy (Bogoyavlenskaya et al. 1991; Braitseva et al. 1991; Turner et al. 2013). The last repose period was from 1000 years BP to 1955 AD (Braitseva et al. 1991; Turner et al. 2013). On 22 October 1955, the first historical eruption of Bezymianny occurred, which ended almost 1000 years of dormancy. A collapse of the southeastern flank of the volcano, due to the intrusion of magma (cryptodome) in its eastern flank, generated a debris avalanche immediately followed by a laterally directed blast on 30 March 1956 (Gorshkov 1959; Belousov 1996; Martel et al. 2025; Ostorero et al. 2025). The 1955–1956 eruption was immediately followed by the quasi-continuous growth of lava domes, with extrusive-explosive behavior, until 1976. From 1977 to the present, extrusive-explosive and effusive periods followed, with phases of more or less extrusion and phases of destruction by lava dome collapse, generating ash clouds and many PDCs; generating block-and-ash flow deposits were often followed by effusions of lava flows (Alidibirov et al. 1990; Turner et al. 2013). These short-lived strong Vulcanian explosive eruptions occurred from the lava dome summit once or twice a year, with ash plumes to heights of 8–15 km (a.s.l.), and with PDCs extending about 12–13 km away from the lava dome (Belousov et al. 2002; Turner et al. 2013). Only a few eruptions during the 1980 s and 1990 s were characterized by effusive activity or lava flows prior to explosions (Belousov et al. 2002; Mania et al. 2019). This style continued until late 2012, and the volcano remained dormant between September 2012 and December 2016. This short period of dormancy ended with the onset of an effusive eruption with lava dome growth (December 2016) and two strong explosive eruptions in March and June 2017 (Mania et al. 2019; Coppola et al. 2021). Thereafter, Bezymianny returned to short explosive eruptions approximately once a year until present, the one in March 2019 being the subject of this study (Davydova et al. 2024).

The explosive eruption in march 2019

This research describes the events and deposits of the explosive eruption on 15 March 2019. The last eruption preceding this event took place on 20 January 2019. This previous eruption started with an explosive phase producing an ash cloud that reached an altitude of 7–9 km, followed by an effusive episode that produced lava flows on the northwestern slope of the lava dome. A detailed account of observational, geophysical, and monitoring data of the volcano related to the March 2019 eruption is given by Girina et al. (2020) and is briefly summarized here:

From February 2019, a thermal anomaly as well as hot avalanches were observed from the crater leading to an aviation warning by the Kamchatka Volcanic Eruption Response Team (KVERT). Hot avalanches became more frequent in early March with the thermal anomaly steadily increasing in temperature. From March 15, ash was recognized in the volcanic plume, extending 100 km northeast of the volcano. The temperature of the thermal anomaly in the summit area began to increase rapidly. At 17:30 UTC on March 15, a strong explosive phase began that produced an ash plume of 12 km height above the crater, and hot avalanches and pyroclastic density currents descended down all slopes of the volcano (Fig. 2). According to estimates by Girina et al. (2020), the explosive phase (VEI 3) lasted about 7.5 h, followed by powerful gas-steam activity for several days. A strong thermal anomaly remained after the explosive phase related to incandescence in the summit area reflecting the discharge of a new lava flow onto the northwestern slope of the lava dome.

Methods

Remote sensing/DEM and UAV data acquisition

High resolution imaging data was acquired before and after the event by satellites and by drones. Specifically, we explore multispectral satellite images acquired by the Sentinel-2 satellites on 11 March 2019 and 16 March 2019. We downloaded the data and used the freely available software package SNAP to combine the bands 7–5-3 to best visualize the distribution of pyroclastic materials on the snow-covered region at a 12 m resolution (Fig. 2). In order to analyze the height variations associated with the 15 March 2019 eruption, we also analyze stereo imagery acquired by Pleiades satellite on 09 September 2018 and 12 October 2020, the data closest bracketing the event and providing a 50 cm resolution dataset. Although this data spans several years of time, it shows localized changes well compared to the overview maps of the Sentinel-2. Pleiades data is acquired in tri-stereo mode, meaning that the same target was photographed in a forward, a nadir, and a backward camera (Shevchenko et al. 2020). We processed the data using Metashape 2.1 to create a bundle adjustment and two point clouds, with 2.5 million points for 2018 and 2.1 million points for 2020, defined in coordinates and height, respectively. From the three-dimensional point clouds, we generated two digital elevation models (DEMs) of ~ 0.5 m resolution. Using a Geoinformatics (GIS) framework (ArcGIS 10.4), we subtracted these DEMs to estimate depositional thicknesses. More information on the Pleiades data, the data availability,

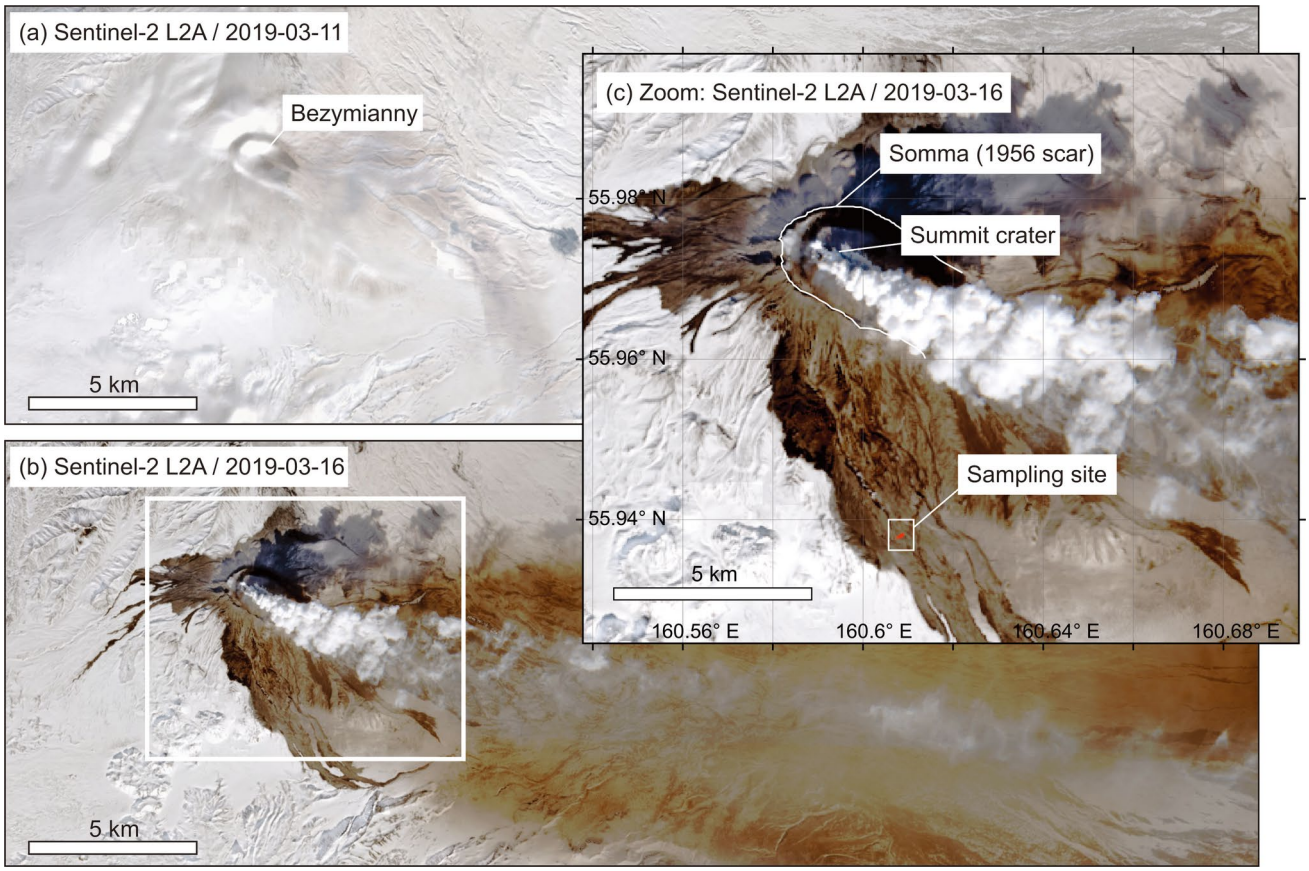

Fig. 2 Natural color satellite images (L2A) from before and after the 15 March 2019 eruption at Bezymianny volcano. **a** Sentinel-2 image on 11 March 2019 showing widespread snow coverage and no activity at Bezymianny. **b** Sentinel-2 image on 16 March 2019 showing dark-brownish colorized terrain associated with airfall, pyroclastic, and lahar deposits. **c** Zoom into the same image as shown in **b**, highlighting the 1956 scar and the site of sampling and drone surveys located 7.2 km SSE of the summit crater. All Sentinel-2 data are freely available from the Copernicus Data Space Environment (https://dataspace.copernicus.eu/)

and processing at Bezymianny volcano can be found in Shevchenko et al. (2020).

To further analyze the characteristics and dimensions of blocks and boulders deposited during the March 2019 event, we performed a fieldwork and drone survey in August 2019. We used a DJI FC 220 camera model aboard a Phantom-4 RTK drone. Referencing was done using the GPS system, so that each image is fully georeferenced. We took 1200 drone images from the pyroclastic deposit; the imagery was also processed using Metashape 2.1, allowing for the generation of a digital elevation model and orthomosaic of 20 and 2 cm, respectively. Using the orthomosaic, we investigated the dimension of these blocks, with results showing histograms of the size versus quantity.

Density, petrography, and mineral analysis

Fresh juvenile samples were collected on the apron of the lava dome within the "amphitheater" collapse structure of Bezymianny. In addition, approximately 10 juvenile scoria samples were collected from the pyroclastic PDC deposits, and one set of samples was taken as a core to rim traverse from one of the large juvenile blocks from the PDC deposit. We also obtained some fresh samples from the active lava dome. Density measurements were done for lava dome samples as well as from several fresh scoria clasts from the juvenile material found in the PDC deposits, following the method by Houghton and Wilson (1989). Sieve analysis of PDC matrix material was done to obtain a grain size distribution of the lapilli and ash-sized fraction (a list with sample localities, density raw data, and GSD is provided as supplementary material S2). Representative samples from different localities were also processed to produce standard petrographic thin sections for observation and documentation with an optical microscope. In addition, high-resolution backscatter (BEI) images were taken from several samples. Fe-Ti oxide mineral compositions were determined by wavelength dispersal spectroscopy (WDS) on a JEOL 8530 F field emission microprobe at Shimane University, Japan. The instrument was operated with a 15 kV accelerating voltage

and a 20 nA current with a 1 µm beam diameter. Counting times were 20 s on the element peak and 10 s on the background. Reference materials were from the Smithsonian Microbeam collection (Jarosewich et al. 1980) with accuracy and precision monitored by the analysis of Smithsonian Ilmenite (NMNH 96189), Chromite (NMNH 117075), and Magnetite (NMNH 114887). Repeated analysis of standard materials usually yields standard deviations of < 0.2 per element oxide wt.%, and accuracy of mineral major element data is also generally very good (Jarosewich et al. 1980).

Results

Deposit characteristics from remote sensing data

The eruption plume was directed towards the east and left a dark trace on the snow-covered landscape, as shown in multispectral satellite imagery (Fig. 2a, b). Dark brownish to black deposits are visible on the snow-covered landscape also on the south, west, and northern flanks of the edifice (Fig. 2c). Material from pyroclastic density currents was distributed over 5 km towards the north, west, southeast, and east, clearly overflowing the 1956 amphitheater rim (Fig. 2c).

On fresh snow, some of the PDCs presumably transformed into small lahars. Towards the south and southeast, more extensive accumulations of PDC deposits formed. The DEMs show that the collapse amphitheater was substantially infilled by the eruption (Fig. 3a-–c), in southern parts leveling out the 1956 scar (Fig. 3d-–f). In proximal areas, material transport occurred largely unconfined, forming a > 50-m-thick accumulation (Fig. 3f) of pyroclastic material within the old collapse remnant and an additional concentric pyroclastic apron beyond the collapse amphitheater rim. This collar of pyroclastic deposits in places overcame the amphitheater headwall and subsequently transformed into channelized flows visible towards the northeastern to southwestern side of the volcano where depositional features were not obscured by congruent ashfalls (cf. Figure 2c). The summit craters also have changed, and a new coulee-type lava dome was emplaced on the summit (Fig. 3e). Some of the thickest deposits (more than 10 m thick) are thus recognizable in the DEM difference near the summit (Fig. 3f), but also in an area 7–8 km further south where a narrow valley was infilled (Fig. 3g-–i). The deposits flattened the relief in the south (Figs. 3g, h and) and left a 100 wide and 14 m thick deposit (insert in Fig. 3i). The same area in the south of Bezymianny was chosen for a detailed UAV photo documentation showing pyroclastic density current deposits (Fig. 4b). These are characterized by multiple flow units with leveed channels and lobate coarse-grained fronts (Fig. 4b). Close-up drone imagery shows that coarse subspherical scoria blocks are widespread (Fig. 4c) and concentrated in the top of the deposit, suggesting they were transported from the top of the flow to the front and then advected to the sides in the flow head (Fig. 4b). Material in the central parts of individual lobes as well as in elevated areas outside the main channel is generally finer-grained and ash-rich.

Granulometry/grain size distribution (GSD)/componentry

Detailed grain size distributions for distal tephra samples as well as matrix samples from proximal PDCs were analyzed by Girina et al. (2020). Here, we add componentry data and grain size distribution (GSD) for the large blocks obtained by analysis of the UAV photomosaic imagery. The overall grain size distribution for the deposit is bimodal and is composed of large blocks visible in drone orthomosaic (Fig. 4c) and abundant fine ash between the blocks, characteristic of block and ash flow deposits. A detailed GSD analysis was done by Girina et al. (2020), and we also determined GSD for one PDC matrix sample (see electronic supplement S2). The large size block fraction itself shows a unimodal GSD with many of the blocks up to or larger than 1 m (insert Figs. 4c and). The deposit is relatively well sorted (see also Fig. 8b–d in Girina et al. 2020). The majority of large blocks (> 90%) are light brown vesicular juvenile material, and only a small fraction is composed of dense grey or reddish oxidized lava blocks. The latter are assumed to be accidental lithic material derived from older lava dome formations or picked up from the slopes of the volcano during transport (Fig. 6b and d). The blocks show a rounded to elliptical geometry, with their long axes arranged perpendicular to the transport direction (Fig. 4c). Larger blocks (> 1 m) commonly show round but oblate shapes (Figs. 4c, 5, and 6c), suggesting sagging and flattening after emplacement, as was observed by Radder et al. (2015).

Petrography, density, and vesicularity

Abundant large juvenile blocks are found throughout the deposit. The shape and textures of these blocks differ from many reported block and ash flow deposits (Miyabuchi 1999; Cole et al. 2002; Charbonnier and Gertisser 2008) but are similar to those described from Tungurahua (Hall et al. 2013; Benage et al. 2014) and Cotopaxi (Rader et al. 2015). In broken-up sections, they resemble pillow lavas in some respects as blocks are subspherical with a glassy rind (Fig. 5 and 6e). In some cases, larger blocks are broken up but remain in situ in a jigsaw fit position, suggesting that breakage occurred after emplacement, presumably cracked by ongoing vesiculation and gas exsolution. Breadcrust textured glassy exteriors are ubiquitous (Figs. 5 and 6), and some parts of the deposit were still cooling during

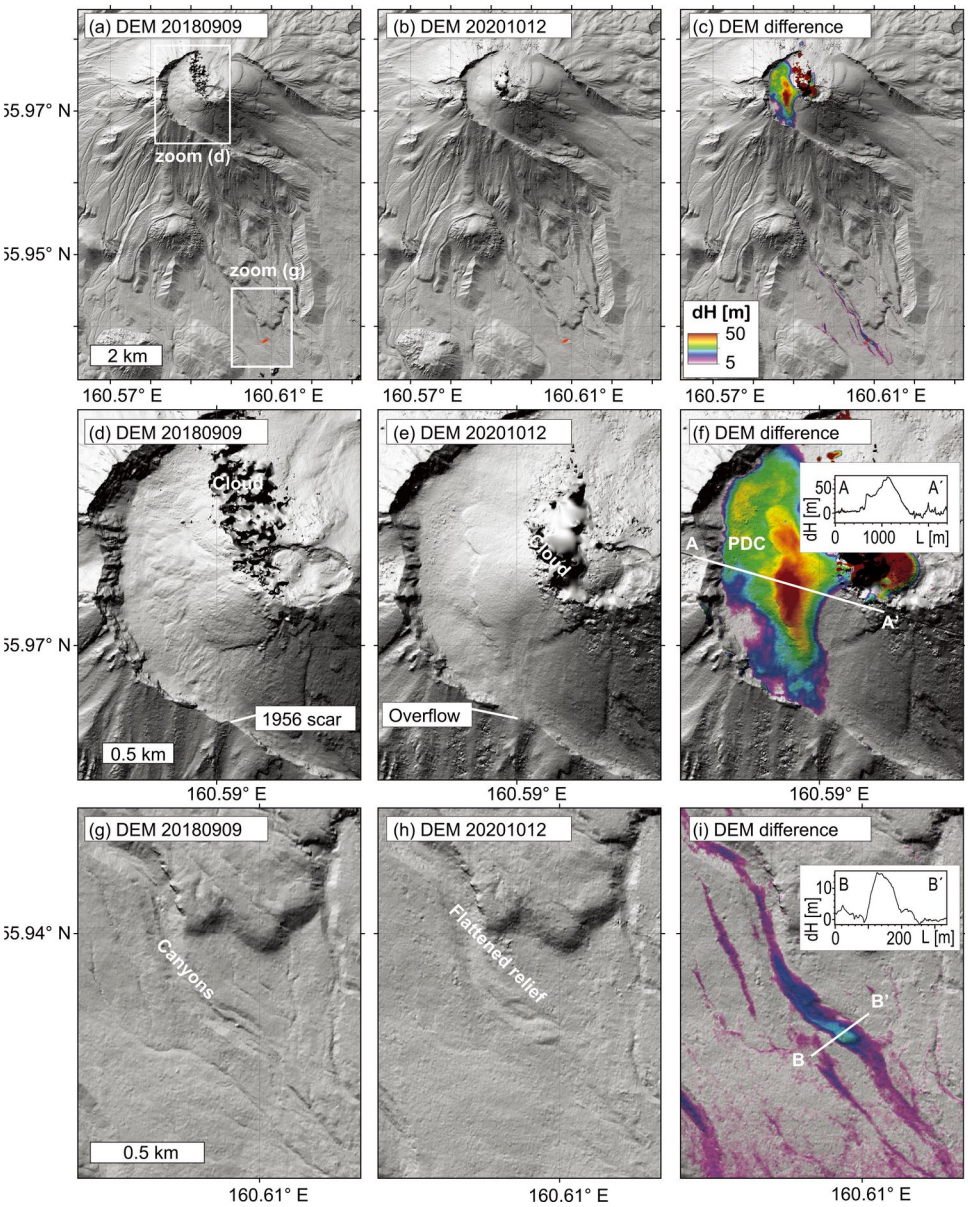

Fig. 3 Shaded relief maps generated from Pleiades tri-stereo satellite data before (left) and after (middle) the March 2019 eruption and difference thereof (right). **a** DEM prior to the eruption. **b** DEM after the eruption. **c** Difference of the DEMs, showing the deposition thickness. **d** Close-up of the summit prior to the eruption and **e** summit after the eruption. **f** Note the infilling of the amphitheater. **g** Close-up of the southern deposition zone prior to the eruption **h** after the eruption. **i** Difference of the DEMs in the southern deposition zone. Insert shows a profile through the data. The data were provided by National Center for Space Studies (CNES) (https://cnes.fr/projets/Plèiades)

our fieldwork (8/2019) and emanating gases from larger blocks. Slickensides on the exterior glassy rinds are common (Fig. 5).

The density of juvenile material from the PDC deposit varies between 0.68 and 1.57 g/cm^3 (Fig. 7). This is significantly lower than those reported from blast deposits, which vary between 1.6 and 2.6 g/cm^3 (Belousov et al. 2007). Densities of the active lava dome rocks have been estimated to be approximately 2.0 g/cm^3 (Zharinov and Demyanchuk 2011). The values obtained from our samples from the active lava dome are also slightly lower (1.45–1.81 g/cm^3). Densities were also analyzed along a transect through one of the large juvenile blocks; however, no systematic density variation was observed within these blocks.

The erupted rocks from the Bezymianny 2019 eruption are hypocrystalline 2-pyroxene andesites with approximately 54–56 wt% silica (Girina et al. 2020). The exteriors of the juvenile blocks are a light-yellow translucent glass (Fig. 8) containing a small number of homogeneous microphenocrysts, mainly plagioclase. Towards the interior of the large blocks, the color of the groundmass glass changes to dark brown. Backscatter images of the interior of larger blocks show incipient crystallization of Fe-Ti oxide and pyroxene nanolites (Fig. 8). Samples from the active lava dome are texturally distinct. They are also hypocrystalline but contain a much larger number of larger normal-zoned plagioclase microphenocrysts (Fig. 8).

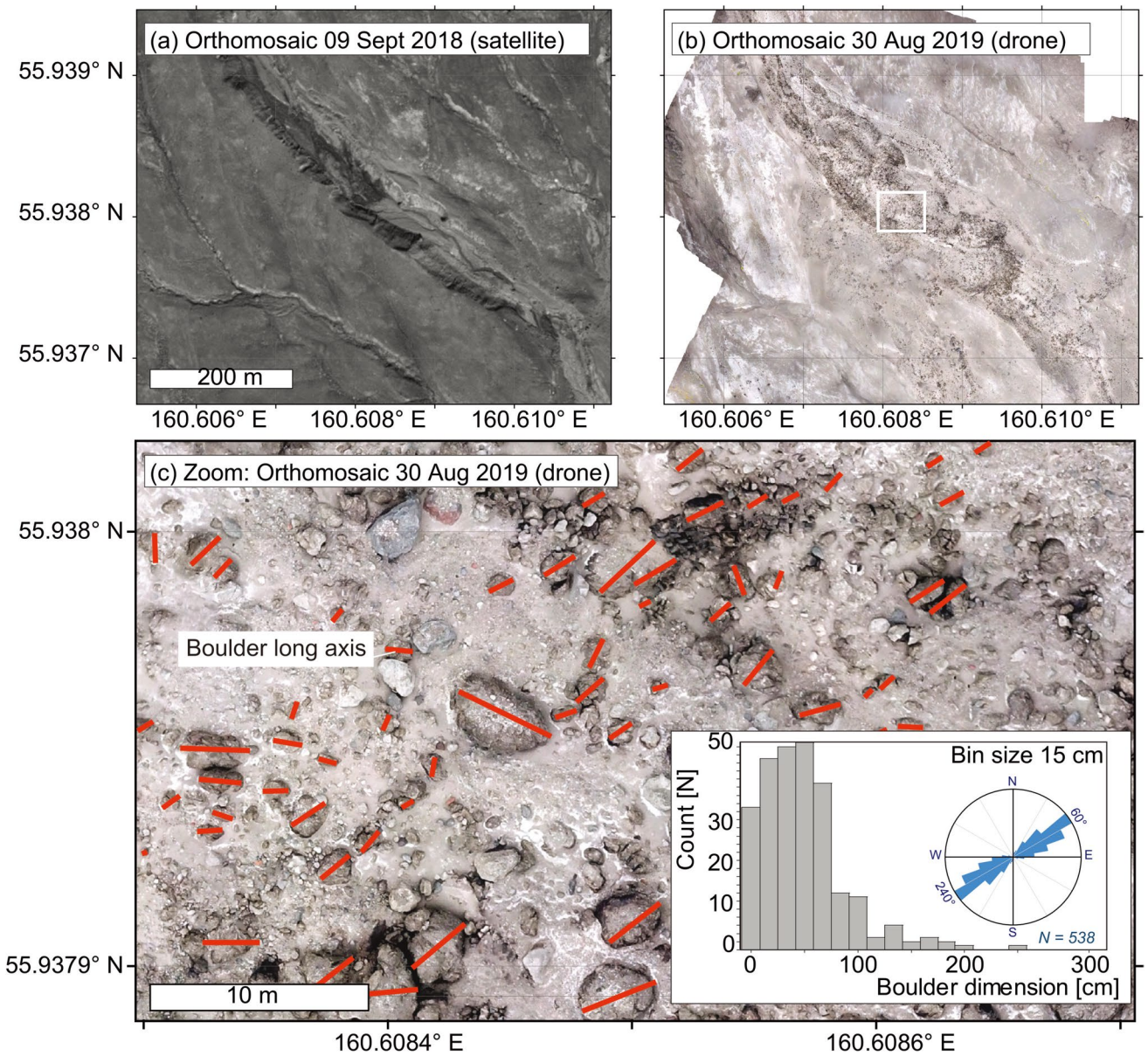

Fig. 4 Southern deposition zone. **a** Satellite Pleiades orthomap prior to deposition shows deep ravines. **b** Drone orthomosaic shows depositional lobes after the eruption. **c** Close-up of the drone orthomosaic revealing the presence of block-and-ash flow deposits. Red lines indicate the long axis of the blocks. Insert shows the Boulder dimension and axis azimuthal distribution of block long axis directions. Block long axes are generally perpendicular to the flow and deceleration direction

Fe-ti oxides

Magmas from Bezymianny volcano contain rhombohedral and cubic Fe-Ti oxides. Textures are different between the lava dome samples and fresh juvenile material from the PDCs (Fig. 9a, b). Thick trellis-type intergrowths between magnetite and ilmenite are ubiquitous in all oxide grains from the active lava dome (Fig. 9c). On the other hand, Fe-Ti oxides from the outer (quenched) glassy rind of large blocks contain no exsolution textures (Fig. 9e). This is true for most of the grains from the interiors of the large blocks. However, in some grains, small, submicrometer incipient lamellae formation can be seen in the exterior rims of some magnetite grains (Fig. 9d).

Compositional range of magnetite–ilmenite pairs is narrow for grains from the juvenile blocks from the PDC (Fig. 9g, Electronic Supplement S3). On the other hand, magnetite–ilmenite compositions from dome samples are highly variable. Two distinct compositional groups of magnetite grains (low and high magnesium) have been identified in samples from the active lava dome and from the block and ash flow (Fig. 9h).

Fig. 5 **a** Surface photograph of the block and ash flow deposit from the March 2019 eruption of Bezymianny volcano. Many of the large blocks contain slickensided friction marks which developed on the outside of many of the large breadcrust blocks (lower two images **b** and **c**)

Discussion

Deposit characteristics

The deposits studied in this work are, according to their bimodal grain size characteristics, block and ash flow deposits. We will discuss the inferred mechanism of PDC initiation and how the type of block and ash flow deposit of the March 2019 eruption is controlled by eruption style at Bezymianny volcano. GSD characteristics of the fine ash matrix of the deposit had previously been studied by Girina et al (2020). Our study adds the GSD for large block-sized material. The ratio between ash-sized material and block-sized material is highly variable within the deposits. Fine-grained ash-rich deposits are mostly found on slopes outside the main channel. Within the main channel, deposits are build up of individual lobes with an overall much higher concentration of large block-sized material, often concentrated in bar-shaped structures (Figs. 4, 5, and 6). Block and ash flow deposits are usually associated with dome collapse processes (Calder et al. 2015). As such, they are also often restricted to a specific sector of the volcano (Ui et al. 1999; Auer et al. 2018; Krippner et al. 2018; Nakada et al. 2019). If the lava dome is located within an amphitheater structure, block and ash flows are commonly channelized down valley from the lowest escarpment of the collapse amphitheater structure (Shevchenko et al. 2020, 2021). The complete snow cover present during the March 2019 eruption suggests that this event distributed material in a broad apron around Bezymianny volcano, leading to substantial accumulation of material within the amphitheater collapse structure but also several kilometers beyond the amphitheater in all directions (Figs. 2 and 3). Beyond this apron, material transported locally often becomes channelized either as PDCs but possibly also locally transforming to lahars due to readily available water from the snow cover. Lava dome and lava flow front collapse has been described previously at Bezymianny (Carter and Ramsey 2009) but usually occurred southeast towards the breach of the collapse amphitheater.

The overall distribution of deposits suggests that the March 2019 PDCs were not derived from lava dome collapse. This idea is supported by the structural properties and petrography of the erupted material. Large juvenile blocks have a lower density than the dome lavas and the vesiculated clasts of the blast deposits (Belousov et al. 2007; Ladygin et al. 2012, 2023), giving them an overall scoriaceous texture (densities of 0.8–1.7 g/cm^3). This makes them comparable to juvenile material described from the deposits of PDCs formed by fountain collapse at Soufrière Hills volcano (Cole et al. 2002), Ngauruhoe

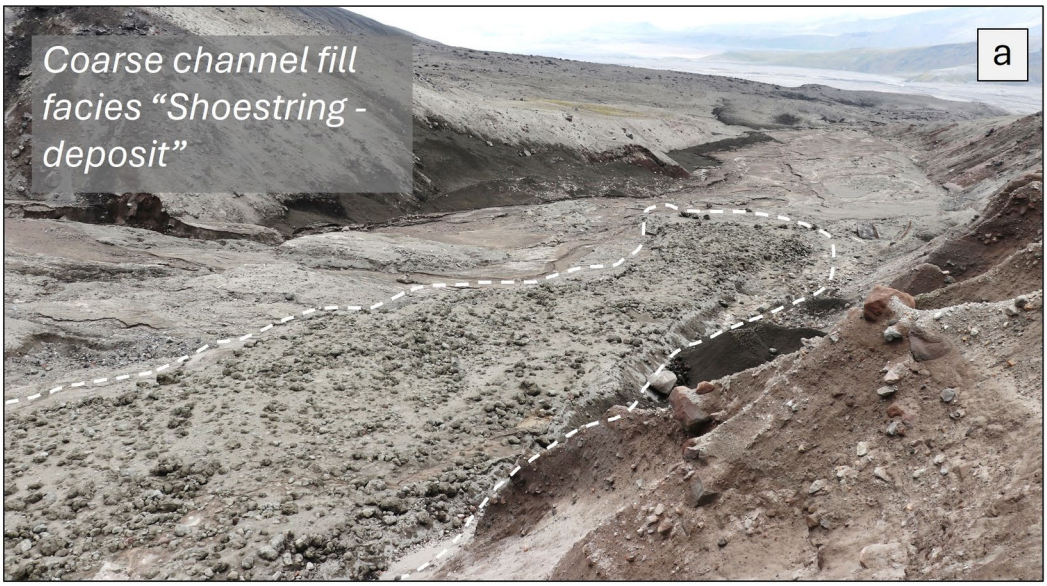
Coarse channel fill facies "Shoestring - deposit"
a

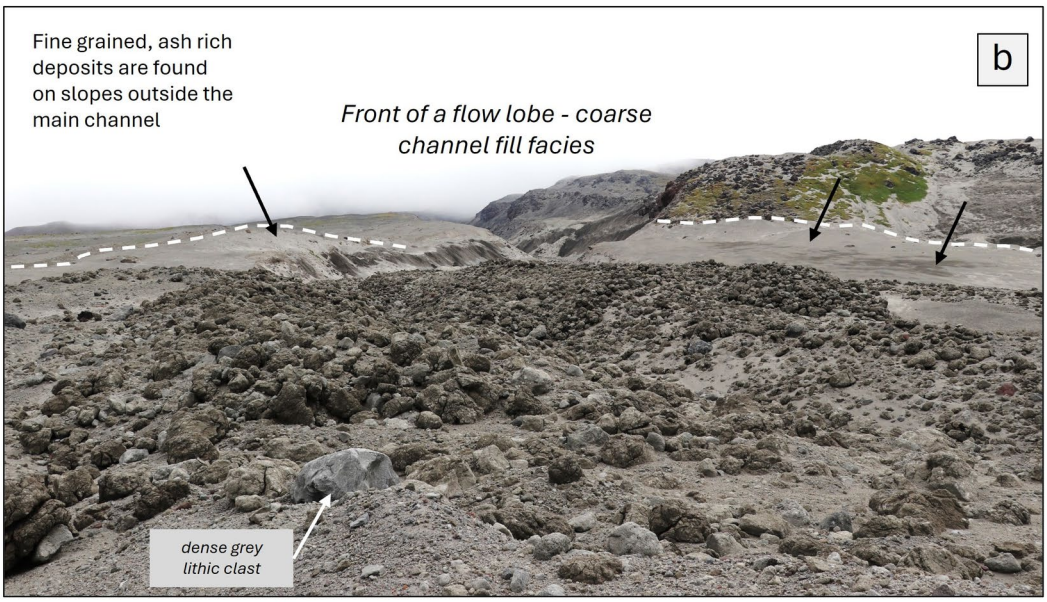
Fine grained, ash rich deposits are found on slopes outside the main channel
Front of a flow lobe - coarse channel fill facies
b
dense grey lithic clast

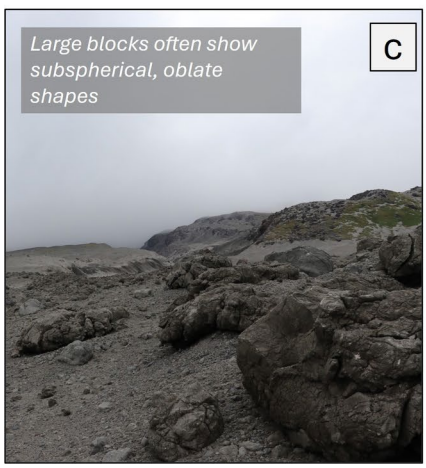
Large blocks often show subspherical, oblate shapes
c

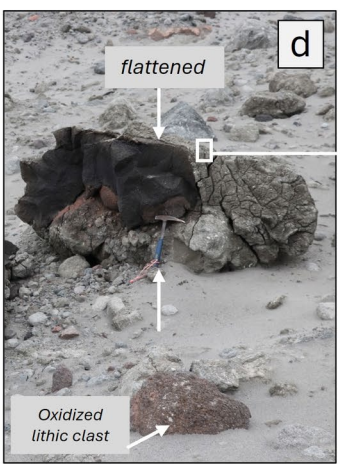
flattened
d
Oxidized lithic clast


Outer glassy rind
e

◂**Fig. 6** Deposits are characterized by distinct coarse "channel fill" deposits **a**, **b**. Individual scoria "breadcrust blocks" can reach several meters in diameter, and friction marks on the exteriors are common. Especially large blocks often show distinct oblate "flattened" shapes, suggesting that blocks had still-viscous interiors after emplacement **c**, **d**. All blocks have a characteristic light brown exterior, glassy rind, and a deep dark brown interior **d**, **e**

volcano (Lube et al. 2007), and Popocatepetl volcano (Macías et al. 2020) which often show equally low densities only slightly above 1 g/cm^3 (Fig. 7). The key difference to the aforementioned examples is the grain size, where studies report significantly smaller block sizes at similar travel distances (ca −6 to −8 phi). In comparison, our UAV GSD for larger blocks reveals a mode over 0.5 m in diameter along with common blocks up to 3 m in diameter. Thus, while the size of individual blocks is comparable to those commonly found in block and ash flow deposits from dome collapse events (Cole et al. 2002), the density is significantly lower than that of lava dome rocks.

Petrography and mineral chemistry provide further evidence that large blocks in the March 2019 PDC are not derived from collapsing portions of the lava dome (Fig. 8). Formation of silica polymorphs is known from active volcanic systems, where volatiles can percolate through permeable upper portions of the magma system with transient storage (Baxter et al. 1999; Boudon et al. 2015; Auer et al. 2024). This has also been documented for high-density lava dome rocks from Bezymianny (Davydova et al. 2022). However, Si-polymorphs have not been found in our juvenile sample material. Exposure of Fe-Ti minerals to atmospheric (P, T) conditions leads to characteristic magnetite–ilmenite exsolution textures, which are common in lava dome rocks and in clasts from block and ash flow deposits derived from the lava dome (Saito et al. 2004, 2007). While these textures are ubiquitous in all Fe-Ti minerals of the studied dome sample (Figs. 8a, c, and e and 9a, c), they are absent in Fe-Ti minerals in the glassy rinds of the breadcrust blocks (Figs. 8b, d and 9b, e). Canil and Lacourse (2020) showed that the trace element composition of magnetite in hydrous silicic magmas is highly susceptible to variations in temperature and oxygen fugacity. Magnesium, in particular, can also be used to distinguish magnetite grains formed in distinct environments. In addition, distinct temperatures for magnetite grains from the glassy rims of large bombs in the block and ash flow (920–964 °C) and the lava dome rocks (737–834 °C) based on the trace element (Mg content in magnetite) geothermometer of Canil and Lacourse (2020) (Fig. 9h) were obtained. A similar range of distinct temperatures can be obtained using the Fe-Ti exchange thermometer of Ghiorso and Evans (2008) for intergrown magnetite–ilmenite grains from the glassy rim of the block and ash flow material (Fig. 9e) and Fe-Ti exsolution lamella (Fig. 9c) within dome rock samples (calculations were done using the ThermoEngine package at the ENKI-portal—http://enki-portal.org/about.html).

Fe-Ti textures together with the glassy crust of all breadcrust blocks and the increasing amount of nanolites towards their interior (Fig. 8d) suggest that each of the individual blocks had a secluded cooling history and is not a disaggregated fragment of a larger lava body. In addition, the ubiquitous flattening of many blocks suggests they were transported and deposited in a ductile state. Similar structures were also described for Cotopaxi samples (Rader et al. 2015). Abundant friction marks on many of the large blocks are similar to those described for block and ash flow deposits from dome collapse events at Soufriere Hills volcano (Grunewald et al. 2000) and Merapi volcano (Schwarzkopf et al. 2001). This shows that block-sized material is transported as fast-moving granular flows where internal mutual interactions between blocks (and also the ground) can exert high stress rates, comparable to those of active faults (Grunewald et al. 2000).

Boiling over eruptions—a useful term?

The deposits and juvenile blocks of the March 2019 eruption of Bezymianny are strikingly similar to those described from the 1877 eruption at Cotopaxi and the 2006 eruption of Tungurahua (Hall et al. 2013; Benage et al. 2014; Rader et al. 2015), with PDCs from both events commonly attributed to a "boiling over" process.

Two general mechanisms have been considered for flow initiation (Dufek et al. 2015): (i) ascending vesiculated magma fragments and vigorously fountains over the crater rim without forming a convective plume, or (ii) vesiculated magma breaches the crater rim as a frothed mass within the open vent and disaggregates under gravity. There are no direct observations of these eruptions, and the crater rims are usually shrouded with ash clouds during such events. The distinction is relevant as it has a bearing on the fragmentation mechanism during the eruption. While low fountaining would still suggest a typical continuous magmatic fragmentation process, the latter is a purely gravitational disintegration of the liquid after leaving the confinement of the crater. However, in neither scenario will magma reach a physical state, and the phase transition of boiling.

For the March 2019 PDC, we interpret the large individual blocks as fragmented pyroclasts with an individual cooling history. Blocks are considered too large to become entrained in a convective plume. Their large size attests to an overall low eruptive energy and fragmentation rate as well as an overall low dispersal. On the other hand, their subspherical shape and the sagging structures suggest ejection in a viscous state. Such an eruption mechanism is therefore an intermediate style between effusive lava dome forming activity and explosive Subplinian to Plinian activity. During

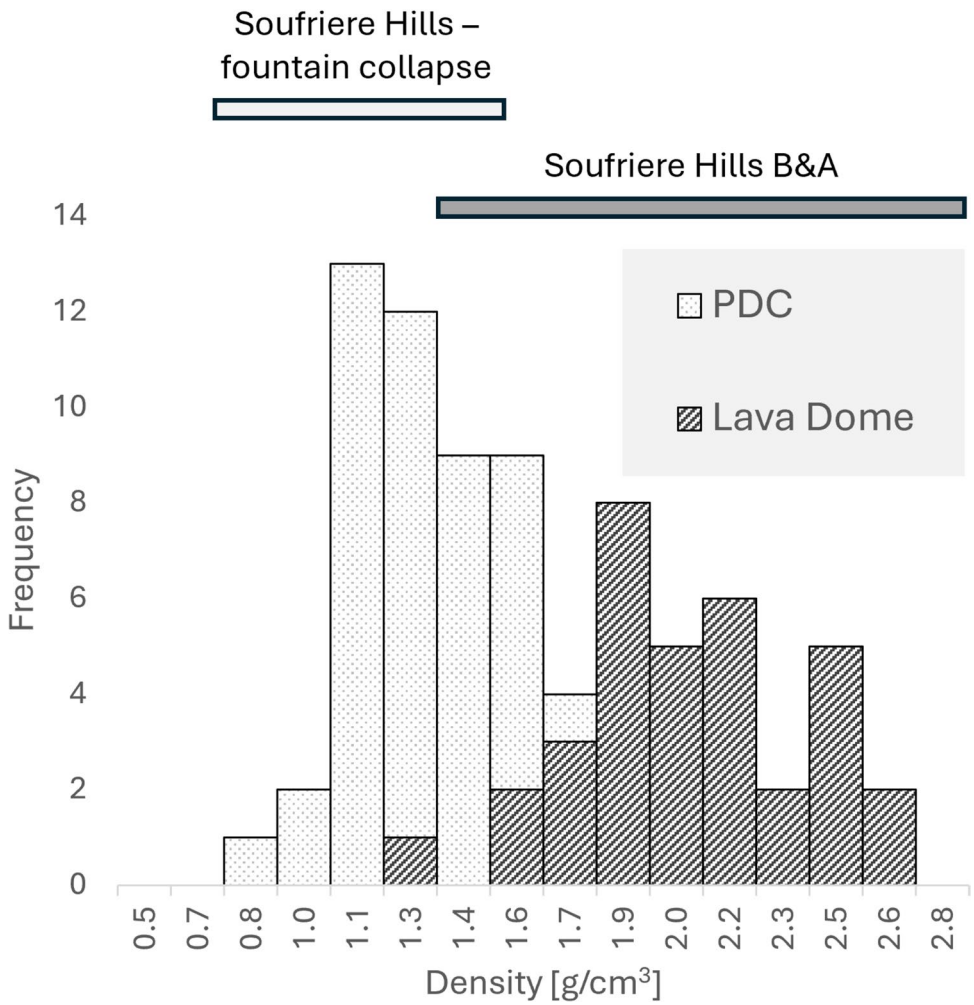

Fig. 7 Comparison of density data for dome rock samples and breadcrust blocks (PDC). Additional data for dome rock densities was taken from Ladygin et al. (2012, 2023). Block and ash flow material and fountain collapse material from the Soufriere Hills Volcano are also shown for reference (Cole et al. 2002)

a lava dome-forming eruption, PDCs are derived from collapsing portions of the lava dome or the front of highly viscous blocky lava flows. On the other side of the spectrum, Subplinian to Plinian activity is characterized by high fragmentation rates and the development of a volcanic plume. In such eruptions, the gas-particle flow emanating from the vent initially starts as a negatively buoyant jet (gas thrust region). During further ascent, it may become buoyant due to heating and entrainment of ambient air, thus decreasing the density of the gas-particle mixture, forming a convective column (Dellino et al. 2014). PDCs form if heating or air entrainment is insufficient, and the jet phase remains denser than the surrounding environment, and the flow collapses. PDCs from explosive activity can also form during fountain collapse following individual Vulcanian explosions (Druitt et al. 2002). The term "boiling over eruption" is engrained in the volcanological literature, but we argue it is a misnomer that poorly describes the processes preceding the initiation of a pyroclastic density current. In the following section, we aim to introduce a more appropriate terminology and interpretation for this eruption type.

Effervescent fountaining—bridging the gap between explosive and lava-dome forming eruptions

Fundamental control on an effusive vs. explosive eruption mechanisms at arc volcanoes with intermediate magma composition are volatile content of the magma as well as gas loss (Martel et al. 1998; Auer et al. 2018), the magma viscosity, ascent rate, and the physical properties of the volcanic conduit (Gonnermann et al. 2013; Cassidy et al. 2018). To interpret the frequently changing eruption mechanism at Bezymianny, we propose a new term *effervescent fountaining* here to describe a mechanism that is transitional between effusive and explosive eruptions. The term eliminates the misconception that magmas reach their boiling point during a volcanic eruption while maintaining the idea that rapid volume expansion due to intense gas exsolution is driving a frothed mass out the conduit. While the 2019 event still produced a large eruption column, the degree of fragmentation and dispersal of large blocks is low. A transition between effusive and explosive eruptions has already been shown

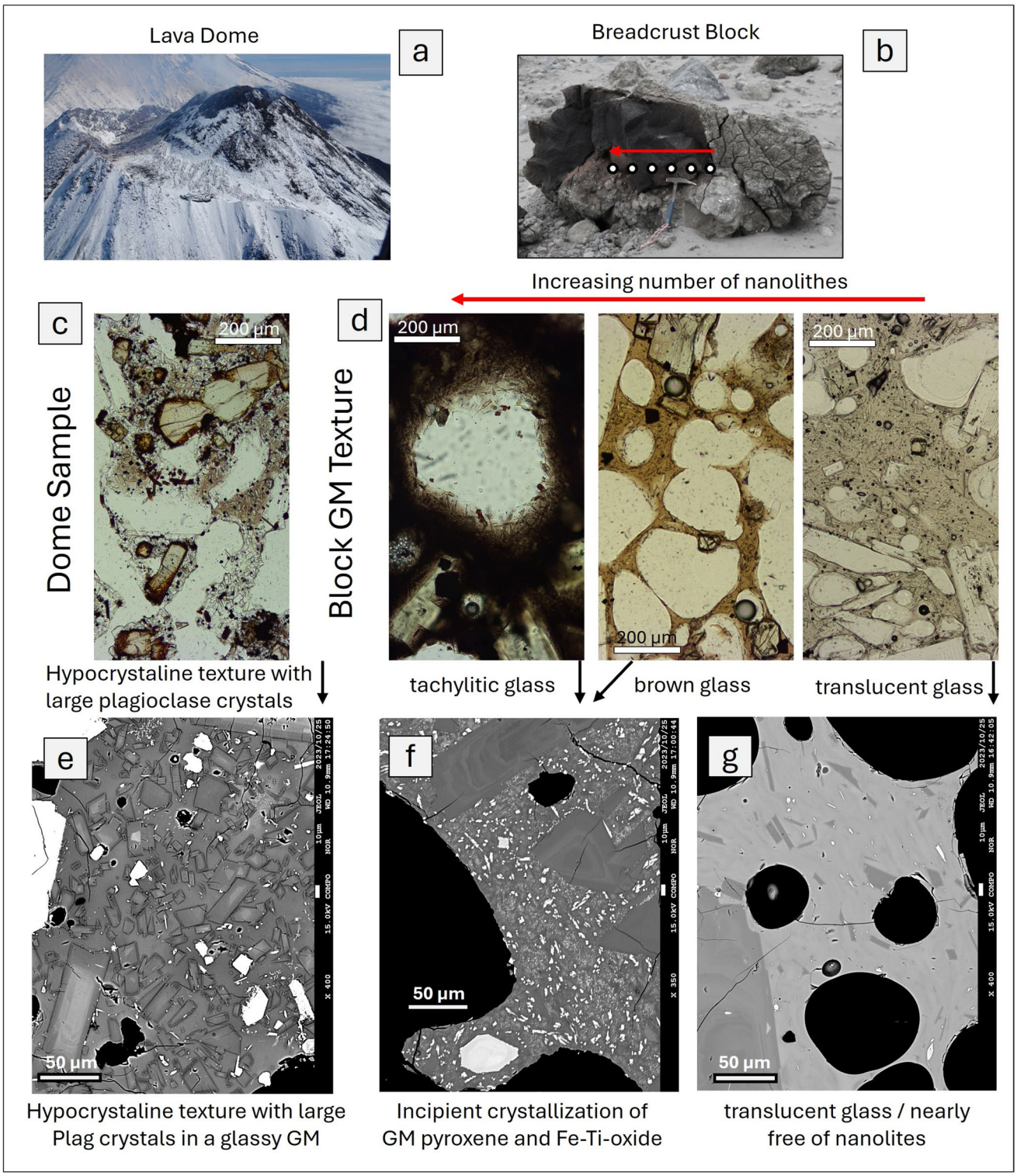

Fig. 8 Groundmass and mineral textures from dome rocks (left side—**a**, **c**, and **e**) and along a traverse through a large breadcrust block (core to rim, right side—**b**, **d**, **f**, and **g**). Dome rocks are hypocrystalline and contain a large number of plagioclase crystals. Breadcrust blocks are characterized by a concentrically increasing number of nanolites towards the interior of the block

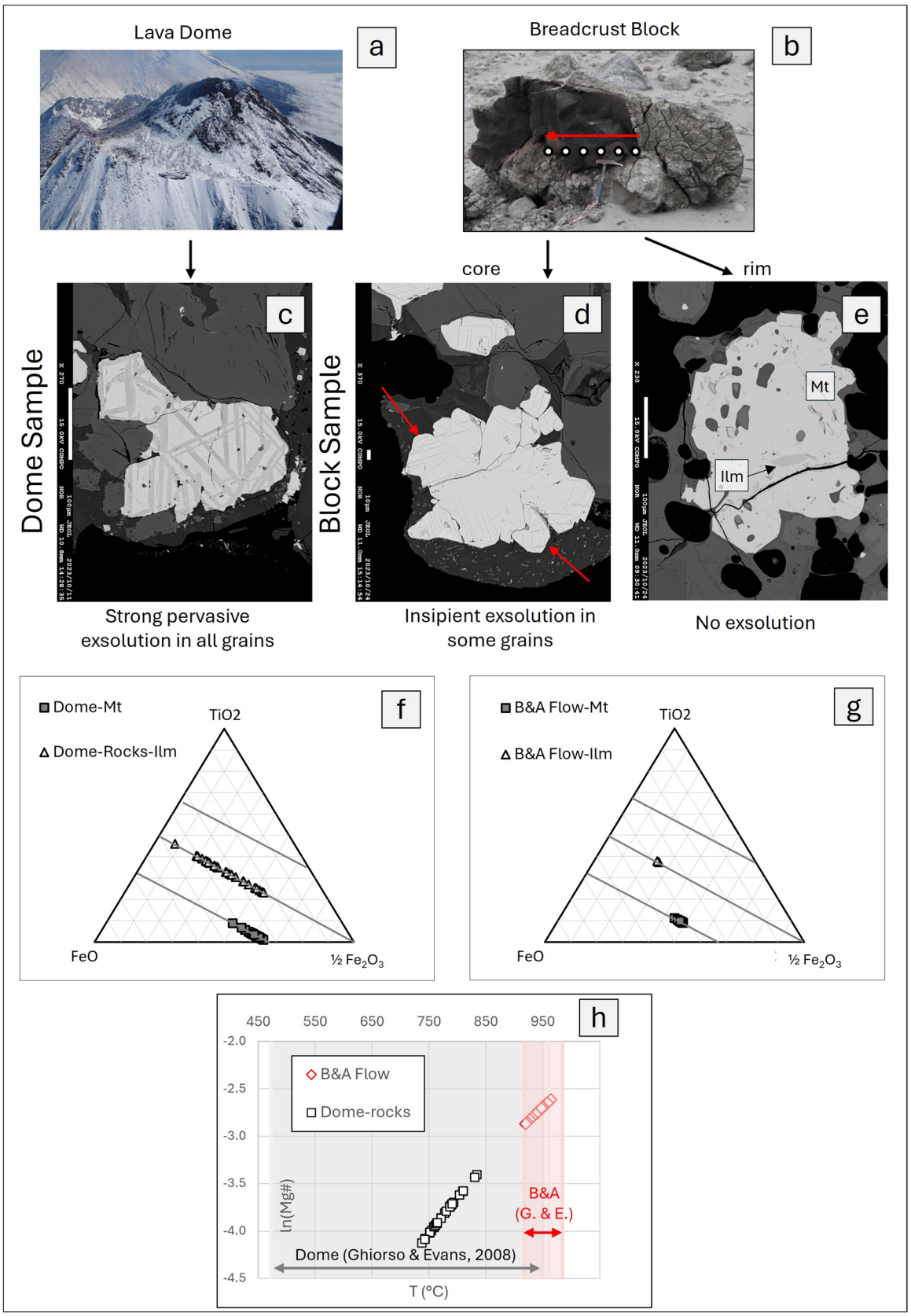
Lava Dome
a
Breadcrust Block
b
core
rim
Dome Sample
Block Sample
c
d
e
Mt
Ilm
Strong pervasive exsolution in all grains
Insipient exsolution in some grains
No exsolution
Dome-Mt
Dome-Rocks-Ilm
TiO2
FeO
½ Fe2O3
f
B&A Flow-Mt
B&A Flow-Ilm
g
450
550
650
750
850
950
-2.0
-2.5
-3.0
-3.5
-4.0
-4.5
B&A Flow
Dome-rocks
ln(Mg#)
B&A
(G. & E.)
Dome (Ghiorso & Evans, 2008)
T (°C)
h

◂**Fig. 9** Fe-Ti mineral composition for dome rocks (left side; **a**, **c**) and through a large breadcrust block (core to rim—right side; **d**, **e**). Below are two triangular diagrams comparing Fe-Ti oxide mineralogy for dome rocks **f** and block and ash flow samples **g**. Diagram **h** shows a distinct temperature range for both sample types based on magnesium content of magnetite (Canil and Lacourse 2020) and magnetite ilmenite Fe-Ti exchange temperature as shaded (grey and red) areas (Ghiorso and Evans 2008)

using numerical modeling for basaltic eruptions where *lava fountaining* represents a separate discrete eruption style that links the two types. Here, the liquid phase in the rising magma remains continuous up to the vent and fragments only at or above the vent level (La Spina et al. 2021). Large juvenile blocks at Bezymianny suggest that the majority of the gas remained coupled to the melt during ascent and fragmentation only occurred at surface levels, where a frothing mass overtops the vent during low fountaining. In the examples described by La Spina et al. (2021), the basaltic fountains feed back into rheomorphic lava flows. No agglutinated deposits were found even in the most proximal areas around the lava dome (which could suggest transformation of ejecta back into lava flows). Instead, the ejected mass at Bezymianny directly feeds into radially dispersed PDCs.

The whole spectrum of eruption styles is present at Bezymianny:

1) *Effusive episodes* (Fig. 10a). These are characterized by predominantly exogenous dome growth of degassed magma. Lava plugs that form frequently in the upper conduit can either lead to episodes of endogenous dome growth but will often be subsequently pushed upward and displaced and integrated into the dome edifice (Mania et al. 2019). Fresh dome material develops Fe-Ti exsolution textures and portions of the lava dome or the flow front can fail generating block and ash flows (Carter et al. 2007; Carter and Ramsey 2009). Material in these deposits is dominated by poorly sorted, dense lava blocks with inherited Fe-Ti exsolution textures.
2) *Effervescent fountaining* (Fig. 10b). During this transitional eruption style, magma strongly vesiculates, but the gas phase does not decouple from the magma which reaches the surface as an effervescent foam. Fragmentation occurs during low fountaining, producing large clasts that do not become entrained in a buoyant plume. These blocks are considered juvenile pyroclasts (sensu stricto) and not remobilized portions of prior emplaced lava. If large volumes of such gas-rich blocks rapidly accumulate on proximal steep slopes, they transform into PDCs that spread out into all directions (Fig. 10b). The resulting deposits are, according to their dominant grain size, block and ash flow deposits; however, the properties of the blocks are distinct from those resulting from lava dome collapse, and their cooling history generates characteristic subspherical juvenile blocks with glassy rims (Benage et al. 2014) that further degas and inflate following deposition (breadcrust blocks).
3) *Explosive episodes* (Fig. 10c). Bezymianny volcano also produces Subplinian and Plinian eruptions (Martel et al. 2025; Ostorero et al. 2025). The fragmentation energy is high, and the fragmentation level is below the surface level, and material reaches the surface as a pyroclastic jet. This represents typical magmatic fragmentation, which, for example, happened in 2023 where a short-lived Subplinian to Plinian eruptive episode produced widely dispersed fallout deposits composed of pumice clasts with densities of < 1 g/cm^3 (Davydova et al. 2024). Such episodes are expected either during the arrival of gas-rich magma at the surface, or after charging the system with gas during prolonged blockage of the crater. In either case, the volume increase due to the expansion of gases and acceleration of the magma supplies sufficient kinetic energy to forcefully eject material from the crater. PDCs are generated via fountain collapse or due to the collapse of an eruption column. Fe-Ti exsolution is expected to be rare as pyroclasts are directly sourced from deeper within the magmatic system but will cool rapidly upon reaching the atmosphere.

Conclusions

We have studied the deposits and erupted materials from the March 2019 eruption of Bezymianny volcano. Due to the complete snow cover prior to the eruption, satellite data allowed for a detailed characterization of material dispersal around the volcano. In addition, a UAV survey obtained high-resolution footage of surface characteristics and basic granulometric data from the deposit. Eruption styles at Bezymianny volcano change rapidly, and such shifts in the eruptive pattern may change material dispersal with strikingly distinct hazard patterns. Initiation mechanisms for PDCs are an important consideration when assessing such hazards. Among the four principal recognized mechanisms, "boiling over" eruptions remain the least studied and least understood. A better understanding may also be inhibited by a long-established but ultimately inappropriate terminology. The deposits we describe are block and ash flows according to their dominant grain size. However, they are not derived from collapsing portions of the active lava dome. Instead, deposit and pyroclast characteristics suggest they were ejected during low fountaining of vesiculated magma. We suggest a number of considerations that could be useful for future studies of similar eruptions and their deposits:

– The term "Boiling over" has been used undifferentiated for relatively small eruptions as discussed in this

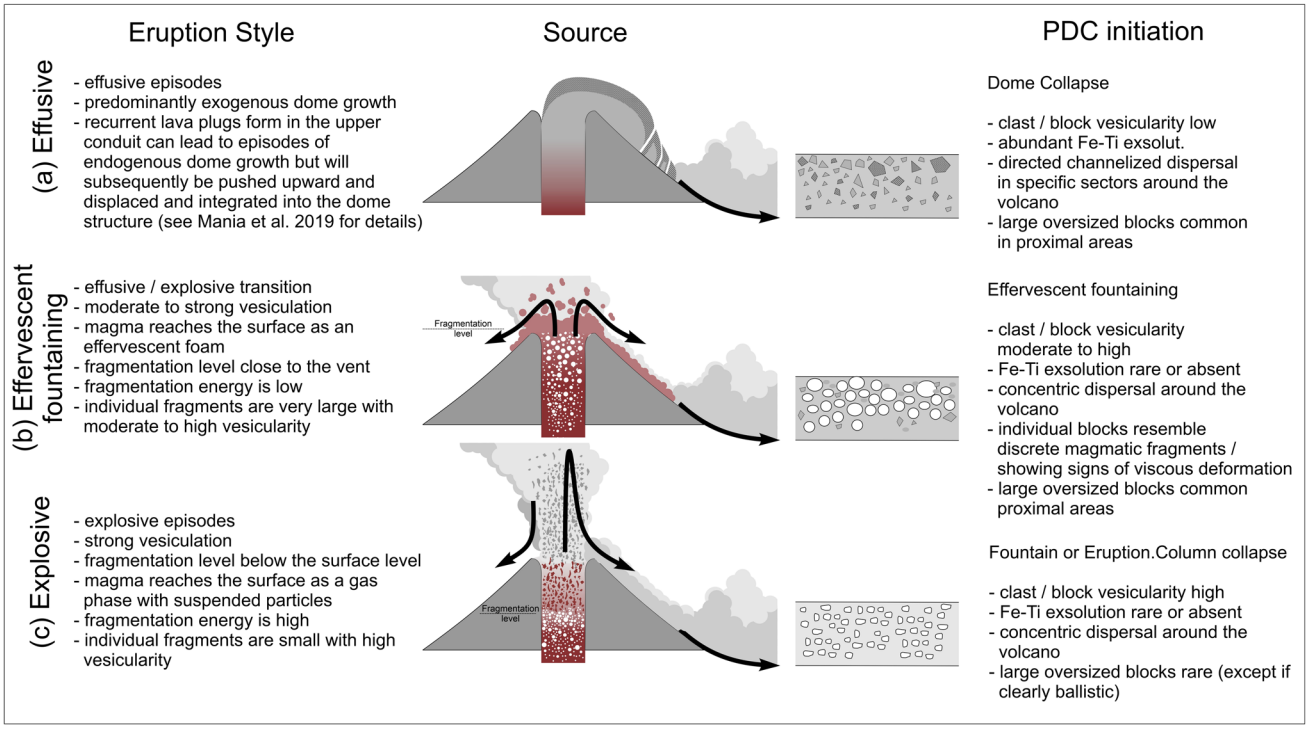

Fig. 10 Spectrum of effusive-explosive eruptions and their relation to PDC initiation as well as the characteristics of deposit and the respective juvenile blocks

work (e.g., Cotopaxi, Tungurahua) and as a model for the emplacement of large Ignimbrite sheets (e.g., Cerro Galán) during Ultraplinian eruption.

– The "Boiling over" eruptions discussed here likely represent a transitional stage between explosive and effusive eruptions
– In analogy to the recent studies on basaltic systems, we think that fountaining is the most appropriate process for this eruption type.
– During ascent, the liquid phase in the rising magma remains continuous up to the vent but also strongly vesiculates with the gas never decoupling from the melt. Magma will fragment at or above vent level vigorously ejecting large block masses of frothed, semi-viscous pyroclasts.
– Such a particulate dispersion of large fragments immediately loses momentum and fails to incorporate with, and heat, sufficient air to become buoyant and will therefore follow fountain-like trajectories to the ground.
– We suggest that "effervescent fountaining" is a more appropriate description of such a process instead of "boiling over."
– Juvenile blocks formed during effervescent fountaining contain glassy rinds suggesting their origin as discrete pyroclasts (Fig. 8d).
– The rapid accumulation of ejecta can initiate PDCs that are not limited to a specific sector of the volcano but are capable of deposition in all directions around the crater (Fig. 2).
– Nevertheless, the resulting deposits can have the textural characteristics of block and ash flow deposits and can contain abundant large, oversized blocks up to several meters in size (Fig. 5a). Thus, the term block and ash flow should not be automatically suggesting a dome collapse origin.
– Juvenile material derived from "effervescent fountaining" is substantially more vesicular than the fragments in block and ash flow deposits derived from collapsing lava flows or lavadomes (Fig. 7).
– Magnetite–ilmenite mineral pairs in "effervescent fountaining" PDCs commonly lack exsolution textures and thus record pristine magmatic conditions. In contrast, material derived from lava domes usually contains these textures (Fig. 9c–e).
– The genetic link between block and ash flows and lava dome collapse processes is deeply engrained in the volcanic literature. Deposits with dominant proportions of large blocks and fine ash that are clearly not of dome collapse origin should simply be termed PDC deposits to avoid confusion.

Supplementary information The online version contains supplementary material available at https://doi.org/10.1007/s00445-025-01868-3.

Acknowledgements We thank editor Olivier Roche and two anonymous reviewers for their constructive comments and suggestions that helped to improve the manuscript. We thank Oleg Chaplygin for samples from the active lava dome and Yuto Müller for help with the density measurements. We acknowledge the Geohazard Supersites and Natural Laboratories Initiative (https://geo-gsnl.org/supersites) and National Center for Space Studies (https://cnes.fr/projets/Plèiades) for providing Plèiades satellite images.

Author contribution A.A., R.M., L.O., G.B., H.B.B., A.B., and M.B. participated in field work in 2019 collecting sample material and characterizing the deposits. R.M. acquired UAV photogrammetric datasets. Photogrammetric data processing and Pléiades satellite data analysis was done by T.R.W. and A.V.S. A.A. analyzed mineral chemistry and wrote the manuscript with contributions of all authors. All authors have read and agreed to the published version of the manuscript.

Funding The field mission in 2019 to Kamchatka (Russia) was funded by the ANR V-Care project (ANR-18-CE03-0010; coordinator: G. Boudon).

Data availability Sentinel-2 data are freely available online by Copernicus Open Access Hub (https://browser.dataspace.copernicus.eu/) and are processed with the free SNAP toolboxes (https://step.esa.int/main/toolboxes/snap/). Pleiades data are collected as a contribution to the GEO-GSNL initiative (https://geo-gsnl.org/supersites/permanent-supersites/kamchatka_kuriles_supersite/) and originally available from Airbus (https://space-solutions.airbus.com/imagery/our-optical-and-radar-satellite-imagery/pleiades/), while Pleiades data products for Bezymianny volcano are available at https://doi.org/10.5880/GFZ.2.1.2020.002.

Declarations

Competing interests The authors declare no competing interests.

References

Alidibirov MA, Bogoyavlenskaya GE, Kirsanov IT, Firstov PP, Girina OA, Belousov AB, Zhdanova EY, Malyshev AI (1990) The 1985 eruption of Bezymiannyi. Volcanology & Seismology 10(6):839–863

Auer A, White JDL, Tobin MJ (2016) Variable H_2O content in magmas from the Tongariro Volcanic Centre and its relation to crustal storage and magma ascent. J Volcanol Geotherm Res 325:203–210. https://doi.org/10.1016/j.jvolgeores.2016.06.021

Auer A, Belousov A, Belousova M (2018) Deposits, petrology and mechanism of the 2010–2013 eruption of Kizimen volcano in Kamchatka, Russia. Bull Volcanol 80:33

Auer A, Belousov A, Belousova M et al (2024) Tridymite formation as a direct consequence of explosive volcanism – evidence preserved in tuffisite veins and concurrently erupted volcanic ash. N Z J Geol Geophys. https://doi.org/10.1080/00288306.2024.2430556

Baxter PJ, Bonadonna C, Dupree R et al (1999) Cristobalite in volcanic ash of the Soufriere Hills Volcano, Montserrat, British West Indies. Science 283:1142–1145

Belousov A (1996) Deposits of the 30 March 1956 directed blast at Bezymianny volcano, Kamchatka, Russia. Bull Volcanol 57:649–662. https://doi.org/10.1007/s004450050118

Belousov A, Voight B, Belousova M, Petukhin A (2002) Pyroclastic surges and flows from the 8–10 may 1997 explosive eruption of Bezymianny volcano, Kamchatka, Russia. Bull Volcanol 64:455–471. https://doi.org/10.1007/s00445-002-0222-5

Belousov A, Voight B, Belousova M (2007) Directed blasts and blast-generated pyroclastic density currents: a comparison of the Bezymianny 1956, Mount St Helens 1980, and Soufrière Hills, Montserrat 1997 eruptions and deposits. Bull Volcanol 69:701

Benage MC, Dufek J, Degruyter W et al (2014) Tying textures of breadcrust bombs to their transport regime and cooling history. J Volcanol Geotherm Res 274:92–107

Bevilacqua A, Bertagnini A, Pompilio M et al (2020) Major explosions and paroxysms at Stromboli (Italy): a new historical catalog and temporal models of occurrence with uncertainty quantification. Sci Rep 10:17357. https://doi.org/10.1038/s41598-020-74301-8

Bogoyavlenskaya GE, Braitseva OA, Melekestsev IV, Maksimov AP, Ivanov BV (1991) Bezymianny Volcano. In Fedotov SA, Masurenkov YUP (eds) Active volcanoes of Kamchatka (vol. 1, pp 195−197) Moscow, Nauka

Boudon G, Balcone-Boissard H (2021) Volcanological evolution of Montagne Pelée (Martinique): a textbook case of alternating Plinian and dome-forming eruptions. Earth-Sci Rev 221:103754

Boudon G, Lajoie J (1989) The 1902 Peléean deposits in the Fort Cemetery of St. Pierre, Martinique: a model for the accumulation of turbulent nuées ardentes. J Volcanol Geotherm Res 38:113–129. https://doi.org/10.1016/0377-0273(89)90033-4

Boudon G, Bourdier J-L, Gourgaud A, Lajoie J (1990) The may 1902 eruptions of Mount Pelée: high-velocity directed blasts or column-collapse nuées ardentes? J Volcanol Geotherm Res 43:359–364

Boudon G, Balcone-Boissard H, Villemant B, Morgan DJ (2015) What factors control superficial lava dome explosivity? Sci Rep 5:14551

Braitseva OA, Melekestsev IV, Bogoyavlenskaya GE, Maksimov AP (1991) Bezymianny: eruptive history and dynamics. J Volcanol Seismol 12:165–194

Branney MJ, Kokelaar BP (2002) Pyroclastic density currents and the sedimentation of ignimbrites. Geological Society of London, p 143

Calder ES, Lavallée Y, Kendrick JE, Bernstein M (2015) Lava dome eruptions. The encyclopedia of volcanoes, second. Elsevier, pp 343–362

Canil D, Lacourse T (2020) Geothermometry using minor and trace elements in igneous and hydrothermal magnetite. Chem Geol 541:119576

Carter AJ, Ramsey MS (2009) Aster-and field-based observations at Bezymianny Volcano: focus on the 11 May 2007 pyroclastic flow deposit. Remote Sens Environ 113:2142–2151

Carter AJ, Ramsey MS, Belousov AB (2007) Detection of a new summit crater on Bezymianny Volcano lava dome: satellite and field-based thermal data. Bull Volcanol 69:811–815. https://doi.org/10.1007/s00445-007-0113-x

Cas R, Wright J (1987) Volcanic successions modern and ancient: a geological approach to processes, products and successions. Springer Science & Business Media

Cassidy M, Manga M, Cashman K, Bachmann O (2018) Controls on explosive-effusive volcanic eruption styles. Nat Commun 9:1–16

Charbonnier SJ, Gertisser R (2008) Field observations and surface characteristics of pristine block-and-ash flow deposits from the 2006 eruption of Merapi Volcano, Java, Indonesia. J Volcanol Geotherm Res 177:971–982

Cole PD, Calder ES, Sparks RSJ et al (2002) Deposits from dome-collapse and fountain-collapse pyroclastic flows at Soufrière Hills Volcano, Montserrat. Geol Soc Mem 21:231–262

Coppola D, Laiolo M, Massimetti F et al (2021) Thermal remote sensing reveals communication between volcanoes of the Klyuchevskoy Volcanic Group. Sci Rep 11:13090

Crandell DR, Hoblitt RP (1986) Lateral blasts at Mount St. Helens and hazard zonation. Bull Volcanol 48:27–37. https://doi.org/10.1007/BF01073511

Davydova VO, Shcherbakov VD, Plechov PY, Koulakov IY (2022) Petrological evidence of rapid evolution of the magma

plumbing system of Bezymianny volcano in Kamchatka before the December 20th, 2017 eruption. J Volcanol Geotherm Res 421:107422

Davydova VO, Kuznetsov RA, Dirksen OV et al (2024) Eruptive products from the Bezymianny volcano eruption of April 7, 2023. J Volcanol Seismol 18:418–431. https://doi.org/10.1134/S0742046324700763

Dellino P, Dioguardi F, Mele D et al (2014) Volcanic jets, plumes, and collapsing fountains: evidence from large-scale experiments, with particular emphasis on the entrainment rate. Bull Volcanol 76:834. https://doi.org/10.1007/s00445-014-0834-6

Druitt TH, Young SR, Baptie B et al (2002) Episodes of cyclic Vulcanian explosive activity with fountain collapse at Soufrière Hills Volcano, Montserrat. Geol Soc Mem 21:281–306

Dufek J (2016) The fluid mechanics of pyroclastic density currents. Annu Rev Fluid Mech 48:459–485. https://doi.org/10.1146/annurev-fluid-122414-034252

Dufek J, Ongaro TE, Roche O (2015) Pyroclastic density currents: processes and models. In: The encyclopedia of volcanoes. Elsevier, pp 617–629

Ghiorso MS, Evans BW (2008) Thermodynamics of rhombohedral oxide solid solutions and a revision of the Fe-Ti two-oxide geothermometer and oxygen-barometer. Am J Sci 308:957–1039

Giordano G, Cas RAF (2021) Classification of ignimbrites and their eruptions. Earth-Sci Rev 220:103697. https://doi.org/10.1016/j.earscirev.2021.103697

Girina OA, Gorbach NV, Davydova VO et al (2020) The 15 March 2019 Bezymianny volcano explosive eruption and its products. J Volcanol Seismol 14:394–409. https://doi.org/10.1134/S0742046320060032

Gonnermann HM, Manga M, Fagents SA (2013) Dynamics of magma ascent in the volcanic conduit. Model Volcan Process Phys Math Volcanism:55–84

Gorshkov GS (1959) Gigantic eruption of the volcano Bezymianny. Bull Volcanol 20:77–109. https://doi.org/10.1007/BF02596572

Grunewald U, Sparks RSJ, Kearns S, Komorowski JC (2000) Friction marks on blocks from pyroclastic flows at the Soufriere Hills volcano, Montserrat: implications for flow mechanisms. Geology 28:827–830

Hall ML, Steele AL, Mothes PA, Ruiz MC (2013) Pyroclastic density currents (PDC) of the 16–17 August 2006 eruptions of Tungurahua volcano, Ecuador: geophysical registry and characteristics. J Volcanol Geotherm Res 265:78–93

Houghton BF, Wilson CJN (1989) A vesicularity index for pyroclastic deposits. Bull Volcanol 51:451–462

Jarosewich E, Nelen JA, Norberg JA (1980) Reference samples for electron microprobe analysis. Geostand Newsl 4:43–47

Krippner JB, Belousov AB, Belousova MG, Ramsey MS (2018) Parametric analysis of lava dome-collapse events and pyroclastic deposits at Shiveluch volcano, Kamchatka, using visible and infrared satellite data. J Volcanol Geotherm Res 354:115–129

La Spina G, Arzilli F, Llewellin EW et al (2021) Explosivity of basaltic lava fountains is controlled by magma rheology, ascent rate and outgassing. Earth Planet Sci Lett 553:116658

Ladygin VM, Girina OA, Frolova YuV (2012) Petrophysical features of lava flows from Bezymyannyi Volcano, Kamchatka. J Volcanol Seismol 6:341–351. https://doi.org/10.1134/S074204631206005X

Ladygin VM, Girina OA, Frolova YuV (2023) The petrophysical properties and strength of extrusive rocks discharged by Bezymianny volcano, Kamchatka. J Volcanol Seismol 17:159–174. https://doi.org/10.1134/S0742046323700197

Lipman PW, Mullineaux DR (1981) The 1980 eruptions of Mount St. Helens, Washington. USGS Rep 1981:577

Lube G, Cronin SJ, Platz T et al (2007) Flow and deposition of pyroclastic granular flows: a type example from the 1975 Ngauruhoe eruption, New Zealand. J Volcanol Geotherm Res 161:165–186

Lube G, Breard ECP, Cronin SJ, Jones J (2015) Synthesizing large-scale pyroclastic flows: experimental design, scaling, and first results from PELE. J Geophys Res Solid Earth 120:1487–1502. https://doi.org/10.1002/2014JB011666

Lube G, Breard EC, Jones J et al (2019) Generation of air lubrication within pyroclastic density currents. Nat Geosci 12:381–386

Macías JL, Arce JL, García-Tenorio F et al (2020) Source and behavior of pyroclastic density currents generated by Vulcanian-style explosions of Popocatépetl volcano (Mexico) on 22 January 2001. J Volcanol Geotherm Res 406:107071

Mania R, Walter TR, Belousova M et al (2019) Deformations and morphology changes associated with the 2016–2017 eruption sequence at Bezymianny volcano, Kamchatka. Remote Sens 11:1278. https://doi.org/10.3390/rs11111278

Martel C, Pichavant M, Bourdier JL et al (1998) Magma storage conditions and control of eruption regime in silicic volcanoes: experimental evidence from Mt. Pelee. Earth Planet Sci Lett 156:89–99. https://doi.org/10.1016/s0012-821x(98)00003-x

Martel C, Erdmann S, Boudon G et al (2025) The 1956 eruption of Bezymianny volcano (Kamchatka)—part I: petrological constraints on magma storage and eruptive dynamics. Bull Volcanol 87:18. https://doi.org/10.1007/s00445-025-01802-7

Miyabuchi Y (1999) Deposits associated with the 1990–1995 eruption of Unzen volcano, Japan. J Volcanol Geotherm Res 89:139–158. https://doi.org/10.1016/S0377-0273(98)00129-2

Nakada S, Zaennudin A, Yoshimoto M et al (2019) Growth process of the lava dome/flow complex at Sinabung Volcano during 2013–2016. J Volcanol Geotherm Res 382:120–136. https://doi.org/10.1016/j.jvolgeores.2017.06.012

Ostorero L, Boudon G, Balcone-Boissard H et al (2025) The 1956 eruption of Bezymianny volcano (Kamchatka). Part II—magma dynamics and timescales from crystal records. Bull Volcanol 87:19. https://doi.org/10.1007/s00445-024-01792-y

Rader E, Geist D, Geissman J et al (2015) Hot clasts and cold blasts: thermal heterogeneity in boiling-over pyroclastic density currents. Geological Society, London, Special Publications 396:67–86

Ruprecht P, Bergantz GW, Cooper KM, Hildreth W (2012) The crustal magma storage system of Volcán Quizapu, Chile, and the effects of magma mixing on magma diversity. J Petrol 53:801–840. https://doi.org/10.1093/petrology/egs002

Saito T, Ishikawa N, Kamata H (2004) Iron–titanium oxide minerals in block-and-ash-flow deposits: implications for lava dome oxidation processes. J Volcanol Geotherm Res 138:283–294

Saito T, Ishikawa N, Kamata H (2007) Magnetic petrology of the 1991–1995 dacite lava of Unzen volcano, Japan: degree of oxidation and implications for the growth of lava domes. J Volcanol Geotherm Res 164:268–283. https://doi.org/10.1016/j.jvolgeores.2007.05.015

Sarocchi D, Sulpizio R, Macías JL, Saucedo R (2011) The 17 july 1999 block-and-ash flow (BAF) at Colima Volcano: new insights on volcanic granular flows from textural analysis. J Volcanol Geotherm Res 204:40–56. https://doi.org/10.1016/j.jvolgeores.2011.04.013

Schwarzkopf L, Schmincke H-U, Troll V (2001) Pseudotachylite on impact marks of block surfaces in block-and-ash flows at Merapi volcano, Central Java, Indonesia. Int J Earth Sci 90:769–775. https://doi.org/10.1007/s005310000171

Shevchenko AV, Dvigalo VN, Walter TR et al (2020) The rebirth and evolution of Bezymianny volcano, Kamchatka after the 1956 sector collapse. Commun Earth Environ 1:15

Shevchenko AV, Dvigalo VN, Zorn EU et al (2021) Constructive and destructive processes during the 2018–2019 eruption episode at Shiveluch volcano, Kamchatka, studied from satellite and aerial data. Front Earth Sci 9:680051

Sparks RSJ, Wilson L, Hulme G (1978) Theoretical modeling of the generation, movement, and emplacement of pyroclastic flows

by column collapse. J Geophys Res Solid Earth 83:1727–1739. https://doi.org/10.1029/JB083iB04p01727

Sparks RSJ, Francis PW, Hamer RD et al (1985) Ignimbrites of the Cerro Galan caldera, NW Argentina. J Volcanol Geotherm Res 24:205–248

Sparks RSJ, Bursik MI, Carey SN, Gilbert JS, Glaze L, Sigurdsson H, Woods AW (1997) Volcanic plumes. John Wiley & Sons Inc

Sulpizio R, Dellino P, Doronzo DM, Sarocchi D (2014) Pyroclastic density currents: state of the art and perspectives. J Volcanol Geotherm Res 283:36–65

Turner SJ, Izbekov P, Langmuir C (2013) The magma plumbing system of Bezymianny Volcano: insights from a 54year time series of trace element whole-rock geochemistry and amphibole compositions. J Volcanol Geotherm Res 263:108–121. https://doi.org/10.1016/j.jvolgeores.2012.12.014

Ui T, Matsuwo N, Sumita M, Fujinawa A (1999) Generation of block and ash flows during the 1990–1995 eruption of Unzen Volcano, Japan. J Volcanol Geotherm Res 89:123–137

Walding N (2022) Exploring pyroclastic density currents with analogue models. Nat Rev Earth Environ 3:499–499. https://doi.org/10.1038/s43017-022-00325-5

Walker G (1973) Explosive volcanic eruptions — a new classification scheme. Geol Rundsch 62:431–446. https://doi.org/10.1007/bf01840108

Wolf T (1878) Der Cotopaxi und seine letzte Eruption am 26. Juni, 1877. Neues Jahrb Miner Geol Palantol 113–167

Zharinov NA, Demyanchuk YuV (2011) Assessing the volumes of material discharged by Bezymyannyi Volcano during the 1955–2009 period. J Volcanol Seismol 5:100–113. https://doi.org/10.1134/S0742046311020072